

Robust linear correlations related to neutron skin thickness

Y. Lei (雷杨),^{1,*} X. Lian (连新),² and C. L. Bai (白春林)^{2,†}

¹*School of Nuclear Science and Technology, Southwest University of Science and Technology, Mianyang 621010, China*

²*College of Physics, Sichuan University, Chengdu 610065, China*

(Dated: March 19, 2025)

We observe various robust linear correlations related to neutron skin thickness (ΔR_{np}) within different interaction ensembles, including newly proposed random Skyrme ensemble. The robust linear correlation between ΔR_{np} , or charge radius difference of mirror nuclei (ΔR_{mirr}), and the isospin asymmetry ($I = \frac{N-Z}{A}$) becomes apparent as the model space is enlarged. Shape coexistence, or shape effect on charge radius, is considered to explain the experimental deviation of $^{18}\text{O}/\text{Ne}$ and some odd- A ΔR_{mirr} s from the $\Delta R_{\text{mirr}} - I$ linearity. The slopes of the linear $\Delta R_{\text{mirr}} - I$ and $\Delta R_{\text{np}} - I$ correlations (C_{np} and C_{mirr} , respectively) are also robustly and linearly correlated to the slope of the symmetry energy (L). These linear correlations are further understood with the similar formulation between L and the symmetry energy coefficient (J). The linear correlations between $C_{\text{np}} - L$ and $C_{\text{mirr}} - L$ are also adopted to constrain L to $20 \sim 36$ MeV with 1σ confidence. Considering the deviation of $^{18}\text{O}/\text{Ne}$ ΔR_{mirr} due to shape coexistence, the 1σ range for L is further narrowed to $28 \sim 36$ MeV, suggesting a relatively soft equation of state for nuclear matter.

I. INTRODUCTION

The nuclear equation of state (EOS) is crucial for understanding the structure of neutron stars [1] and the dynamical processes in binary compact-star mergers and core-collapse supernovae. These events provide conditions of high densities and temperatures, essential for nucleosynthesis beyond the iron group [2]. Additionally, the density dependence of the nuclear symmetry energy within the EOS plays a significant role in studying drip lines, nuclear masses, and collectivities of neutron-rich nuclei [3–11].

The neutron skin thickness, ΔR_{np} , defined as the difference between the root-mean-squared radii of the neutron and proton density distributions. It represents a delicate equilibrium between the inward pressure arising from surface tension and the outward pressure due to degeneracy. This equilibrium is reminiscent of the one found in neutron stars, albeit with the inward pressure stemming from gravity in that context. Consequently, the bulk properties of neutron stars are likely related to the neutron skin of nuclei [12–18].

Specifically, ΔR_{np} is believed to be positively and linearly correlated with the parameter L [19–21], which represents the slope of the symmetry energy against nucleon density at saturation density ρ_0 . L plays a pivotal role in extending our understanding to high-density scenarios, where unique astrophysical objects and events may potentially exist and manifest themselves [22]. For neutron stars, L —indicating the softness or stiffness of the EOS—determines their radius [1]. In symmetric nuclear matter, L is proportional to the pressure of pure neutron matter at ρ_0 [23]. However, L cannot be directly measured experimentally, so data from terrestrial nuclear laboratory

experiments and astrophysical observations are used to constrain it. Various studies have reported different constraints for L , such as 88 ± 25 MeV from isospin diffusion data in heavy-ion collisions [24], 58.9 ± 16 MeV from 29 previous analyses [25], 58.7 ± 28.1 MeV from averaging over more than 53 results [26], 59.8 ± 4.1 MeV using a Bayesian approach [27], 57.7 ± 19 MeV from neutron-star observations following the binary neutron star merger GW170817 [28], $50.3 \sim 89.4$ MeV and $29.0 \sim 82.0$ MeV from the pygmy dipole resonance of ^{68}Ni and ^{132}Sn , respectively [29], and 37 ± 18 MeV from isovector giant quadrupole resonance energies [30]. Admittedly, not all experimental data could be included here. Nevertheless, given these varying constraints from different data sources, it remains an open question whether L is smaller or larger, implying a softer or stiffer EOS, and correspondingly, smaller or larger neutron star radii.

Obviously, the correlation between ΔR_{np} and L is also valuable for constraining L through nuclear radius measurements. The basic approach involves constructing an ensemble within a specific many-body theory framework (typically the Skyrme-Hartree-Fock model or covariant energy density functional theory), where different interaction or energy density functional parametrizations are applied to a nucleus with an experimentally determined ΔR_{np} . Within this ensemble, a quantitative correlation between ΔR_{np} and L is anticipated. Consequently, experimental values of ΔR_{np} can offer constraints on L . Many studies have been conducted along this line of thinking [31–36].

However, measuring the neutron radius is more difficult and less accurate than measuring the proton radius because experimentalists are more adept at manipulating electromagnetic interactions, suitable for proton exploration, than strong or electroweak probes sensitive to neutron density. Therefore, an alternative to ΔR_{np} for constraining L is desirable. Wang, Li, and Brown proposed that the charge radii difference between mirror nuclei (ΔR_{mirr}) should also be correlated with

* leiyang19850228@gmail.com

† bclphy@scu.edu.cn

L , considering that under nuclear isospin conservation, $\Delta R_{\text{mirr}} \simeq \Delta R_{\text{np}}$ [16, 37]. Since ΔR_{mirr} only involves proton density probes, it may provide more precise data for constraining L . Studies using mirror nuclei have deduced L values within various ranges [38–40], and a recent comprehensive survey further identified some mirror pairs that may be less suitable for L calibration, and emphasized the pairing effect in weakening the correlation between ΔR_{mirr} and L [41].

Furthermore, a linear correlation between $\Delta R_{\text{np}}/\Delta R_{\text{mirr}}$ and the isospin asymmetry $I = \frac{N-Z}{A}$ has been noted [42–44]. As shown in Figure 1, except for ΔR_{mirr} of the $^{18}\text{O}/\text{Ne}$ pair, all recently measured data for even-even nuclei follow this general linear correlation. The liquid drop model is often used to explain this linear relationship [21]. It has also been explained and reproduced by mean field, *ab initio* coupled cluster, and auxiliary field diffusion Monte Carlo models [44–48].

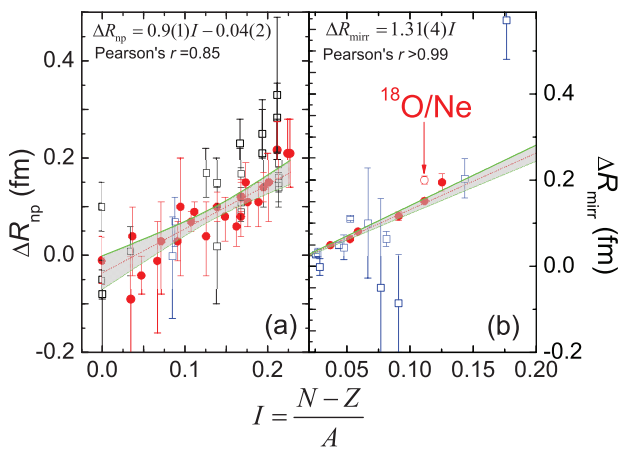


FIG. 1. (Color online) Experimental ΔR_{np} and ΔR_{mirr} against $I = \frac{N-Z}{A}$, in Panel (a) and (b), respectively. For each nucleus, the most recent data available to us are shown as red filled circles (\bullet) for even-even nuclei and blue open boxes (\square) for odd-mass nuclei. In Panel (a), recent data are taken from Refs. [49–53], and other ΔR_{np} data from Refs. [49–51, 54–58] are represented by black open boxes (\square). It can be seen that the recent ΔR_{np} data suggests a linear trend with I , characterized by a Pearson correlation coefficient of $r \simeq 0.85$. For the recent ΔR_{np} data, a linear fit was performed, yielding $\Delta R_{\text{np}} = 0.9(1)I - 0.04(2)$, indicated by the gray shaded 1σ -confidence band. In Panel (b), ΔR_{mirr} data are from Ref. [39, 42, 59–61], and a strong linear correlation is observed, with a Pearson correlation coefficient $r > 0.99$ for even-even nuclei, except for the $^{18}\text{O}/\text{Ne}$ mirror pair. Therefore, the data for $^{18}\text{O}/\text{Ne}$ is highlighted by red open circles (\circ). For this general linear correlation, a proportional fit was performed, constrained by $\Delta R_{\text{mirr}} \equiv 0$ at $I = 0$. This fitting yields $\Delta R_{\text{mirr}} = 1.31(4)I$, indicated by the gray shaded 1σ -confidence band. We also note that the systematics of odd-mass ΔR_{mirr} data shows more scatter, which will be discussed in Sec. IV B, along with the deviation of the $^{18}\text{O}/\text{Ne}$ mirror pair.

Consequently, a many-body theory, when based on appropriate parameters related to L and capable of yielding

experimentally consistent ΔR_{np} or ΔR_{mirr} values for nuclei with available data, might be expected to exhibit this linear correlation between ΔR_{np} (or ΔR_{mirr}) and the isospin asymmetry $I = \frac{N-Z}{A}$, with a slope and intercept that align with experimental findings. Therefore, the existence, slope, and intercept of this linear correlation within a many-body framework could potentially offer constraints on L , by considering the available experimental ΔR_{np} or ΔR_{mirr} data.

A key question is whether the linear correlation between ΔR_{np} (or ΔR_{mirr}) and the isospin asymmetry $I = \frac{N-Z}{A}$ persists in many-body theory ensembles, even without finely tuned Hamiltonians or Lagrangians related to reasonable L s. It is worth noting that many-body calculations [44–48] that reproduce this linear trend employ diverse interactions, model spaces, and even theoretical frameworks. This observation might suggest that this correlation could be largely independent of interaction and modeling details, indicating a degree of robustness. However, such linearity is not necessarily guaranteed, at least from a microscopic perspective. Therefore, it is pertinent to investigate if this correlation is indeed a robust, simple feature emerging from the complex many-body system, or if it relies on specific or sophisticated nucleon-nucleon interactions.

Nuclear robust properties can be effectively explored within a random interaction ensemble of nuclear structure models [62–65], where all two-body (and even one-body) interaction matrix elements are assigned random values. Using random interactions, one can perform many-body calculations repeatedly. Statistical analysis of these calculations reveals how *simple* regularities can emerge from *complex* nuclei, even when employing interactions significantly different from realistic interactions [66]. Examples of such regularities are the predominance of $I^\pi = 0^+$ ground states [67, 68], the collective-like motions [69, 70], odd-even staggering in proton-neutron interactions [71], and robust correlations among nuclear observables [72, 73].

This work employs the idea of random interactions to explore potential robust correlations between ΔR_{np} , ΔR_{mirr} , I , L , and related quantities. Section II discusses the robustness of the linear relationships between ΔR_{np} and I , as well as ΔR_{mirr} and I , using the shell model and the Skyrme-Hartree-Fock (SHF) model. Section III shows that the slopes of the $\Delta R_{\text{np}} - I$ and $\Delta R_{\text{mirr}} - I$ linear relationships also exhibit a robust linear correlation with L . An analytical explanation is presented. Section IV utilizes the slopes of the $\Delta R_{\text{np}} - I$ and $\Delta R_{\text{mirr}} - I$ linear relationships to constrain L , considering the shape coexistence in $^{18}\text{O}/\text{Ne}$. The influence of nuclear shape on the $\Delta R_{\text{mirr}} - I$ relationship is emphasized, and this is used to explain the off-systematics behaviors observed in odd- A ΔR_{mirr} . Section V summarizes this work.

II. $\Delta R_{\text{np}} - I$ AND $\Delta R_{\text{mirr}} - I$ LINEARITY

A. random quasi-particle ensemble (RQE)

To examine the robustness of the linear relationship between ΔR_{np} (or ΔR_{mirr}) and I , several considerations were taken into account before performing the random interaction calculations.

First, we need to decide which random-interaction ensemble to adopt. We chose to use the random quasi-particle ensemble (RQE) [67] without isospin symmetry. In the RQE, the statistics of two-body interaction matrix elements is invariant under particle-hole transformation. This ensures consistent interaction statistics govern shell-model calculations within the model space, facilitating a wider range of accessible I in the RQE.

Second, we need to consider the model space for RQE calculations. Many-body calculations within a single major shell of the harmonic oscillator always yield a constant expectation value for the \hat{r}^2 operator, resulting in zero ΔR_{np} . With two adjacent major shells, $\langle \hat{r}^2 \rangle$ becomes a linear combination of particle occupations across the two shells, which might lead to a trivial linear correlation between ΔR_{np} (or ΔR_{mirr}) and I . From a microscopic perspective, the nonlinear contribution to ΔR_{np} is expected to arise from one-body correlations across two major shells, specifically, the non-zero off-diagonal matrix elements of $\langle nl|r^2|n'l \rangle$. For nuclei heavier than those of the sd shell, this nonlinear contribution may be negligible. To investigate the influence of nonlinear contributions from off-diagonal matrix elements on the linearity of $\Delta R_{\text{np}} - I$ and $\Delta R_{\text{mirr}} - I$ correlations, our shell-model calculations are performed within a single-particle model space including single-particle orbits from two major shells but restricted to the same orbital angular momentum l and total angular momentum j . Specifically, we perform our RQE calculations in spaces of $\{1d_{5/2}, 2d_{5/2}\}$, $\{1f_{7/2}, 2f_{7/2}\}$, $\{1h_{9/2}, 2h_{9/2}\}$, $\{1h_{11/2}, 2h_{11/2}\}$, $\{1j_{13/2}, 2j_{13/2}\}$, and $\{1j_{15/2}, 2j_{15/2}\}$, denoted by $d_{5/2}$, $f_{7/2}$, $h_{9/2}$, $h_{11/2}$, $j_{13/2}$ and $j_{15/2}$ model spaces in this paper.

Third, using the RQE, we repeatedly perform over 1000 shell-model calculations for each calculable* pseudo nucleus in these model spaces. For a pseudo nucleus with Z protons and N neutrons, the expectation values of \hat{r}^2 for the resulting ground states are calculated for both proton and neutron distributions, denoted as $\langle \hat{r}_\pi^2 \rangle(Z, N)$ and $\langle \hat{r}_\nu^2 \rangle(Z, N)$, respectively. The squared charge radius $r_{\text{ch}}^2(Z, N)$ is calculated based on the method described in Ref. [61]. Thus, we define $\Delta R_{\text{np}}(Z, N) = \sqrt{\langle \hat{r}_\nu^2 \rangle(Z, N)} - \sqrt{\langle \hat{r}_\pi^2 \rangle(Z, N)}$, and $\Delta R_{\text{mirr}}(Z, N) = \sqrt{r_{\text{ch}}^2(N, Z)} - \sqrt{r_{\text{ch}}^2(Z, N)}$. Further-

more, we calculate the Pearson's r coefficient [75] between $\Delta R_{\text{np}}(Z, N)$ (or $\Delta R_{\text{mirr}}(Z, N)$) and $I = \frac{N-Z}{A}$ for each random interaction. In this context, $|r| = 1$ indicates perfect linearity, while $|r| = 0$ implies no linear correlation between the radius differences and isospin asymmetry I . Subsequently, we count the occurrences of $|r|$ in each model space. The probabilities of $|r| > 0.95$, $P(|r| > 0.95)$, are then shown in Fig. 2 against the model-space sizes, which correspond to the maximum nucleon number in each model space.

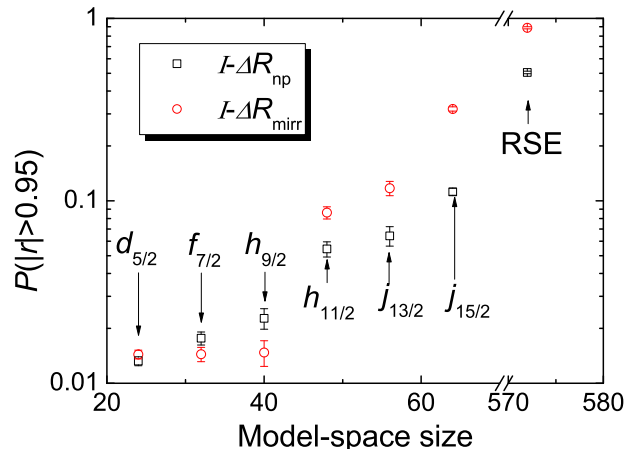


FIG. 2. (Color online) Probabilities of Pearson's $|r| > 0.95$, $P(|r| > 0.95)$, for $\Delta R_{\text{np}} - I$ and $\Delta R_{\text{mirr}} - I$ correlations, against model-space sizes within the RQE (random quasi-particle ensemble) and RSE (random Skyrme ensemble) calculations. For RQE, corresponding model-spaces are labeled. The error bar corresponds to the statistic error of $|r|$ counting. According to our numerical test, if our many-body calculations provided independent random number as ΔR_{np} and ΔR_{mirr} output, there would have been normally less than 10^{-5} order of possibility to produce $|r| > 0.95$, i.e., we would not have observed a single linear correlation within 10000 random-interaction runs.

As shown in Fig. 2, our RQE calculations indicate that linear $\Delta R_{\text{np}} - I$ and $\Delta R_{\text{mirr}} - I$ correlations with $|r| > 0.95$ occur with a probability greater than 1%. This probability suggests a notable predominance of these linear correlations within the RQE framework. This is particularly significant considering that the probability of achieving $|r| > 0.95$ would typically be on the order of 10^{-5} if our shell-model calculations were to produce independent random numbers as outputs for ΔR_{np} and ΔR_{mirr} , as demonstrated by our numerical tests.

We also observed that as the model space size increases, the probability $P(|r| > 0.95)$ increases significantly for both $\Delta R_{\text{np}} - I$ and $\Delta R_{\text{mirr}} - I$ correlations. This suggests that the linearity of these correlations becomes more pronounced with increasing model space size. This trend appears to be more evident for the $\Delta R_{\text{mirr}} - I$ correlation.

* Note: "Calculable" means the shell-model calculation for a specific pseudo nuclei takes no more than 64GB memory with a 36-thread openmp run of BIGSTICK [74].

B. random Skyrme ensemble (RSE)

Due to the computational demands of shell-model calculations, the model space in RQE calculations is limited. To extend our investigation, we employ Skyrme-Hartree-Fock (SHF) calculations using the lowest 10 major shells of an isotropic harmonic oscillator. This significantly expands our model space to 572 single-particle levels, considerably larger than those employed in our RQE calculations. These SHF calculations were performed using the HFBTHO code [76], with zero-range pairing interactions disabled. This is because pairing interactions can generally weaken the linear correlation between ΔR_{mirr} and L [41]. We also used a prolately deformed initial basis with $\beta = 0.2$, as most of deformed nuclei tend to exhibit prolate shapes.

For these calculations, we collected 160 previously proposed Skyrme parametrizations, primarily from Ref. [77]. We then performed SHF calculations for all even-even nuclei shown in Fig. 1, as well as ^{22}Si , ^{26}S , ^{30}Ar , ^{34}Ca , ^{38}Ti , ^{28}S , and ^{50}Ni . The latter nuclei were included to broaden the range of I in our investigation of the linear correlation of $\Delta R_{\text{mirr}} - I$, as in Ref. [44]. In this paper, we focus on even-even nuclei because odd- A ΔR_{mirr} values can deviate substantially from the general $\Delta R_{\text{mirr}} - I$ linear trend, as seen in Fig. 1. Furthermore, many-body calculations for odd- A nuclei are considerably more complex due to the unpaired nucleon. This set of calculations constitutes what we term the ‘‘Skyrme ensemble’’.

Within this Skyrme ensemble, we observed a clear linear correlation between $\Delta R_{\text{np}} - I$ and $\Delta R_{\text{mirr}} - I$ with Pearson’s $r > 0.85$ for *all* considered parametrizations. This is consistent with experimental observations depicted in Fig. 1. We also noticed that the probability of achieving $r > 0.995$ for $\Delta R_{\text{np}} - I$ linearity is 5%, which is notably smaller than the 69% observed for $\Delta R_{\text{mirr}} - I$ linearity. This suggests that, within the Skyrme ensemble, Pearson’s r values for the $\Delta R_{\text{np}} - I$ correlation are generally lower than those for the $\Delta R_{\text{mirr}} - I$ correlation. This is in line with our RQE findings in Fig. 2, suggesting that the linearity of the $\Delta R_{\text{mirr}} - I$ correlation may become more prominent with larger model spaces.

Such a high probability of obtaining r values close to 1 might indicate a possible interaction-independent property of quantum many-body systems described by Skyrme forces. Thus, we proceeded to further randomize the Skyrme parametrizations. A typical Skyrme force is characterized by 10 parameters ($t_{0\sim 3}$, $x_{0\sim 3}$, W_0 and $1/\sigma$), as detailed in Eq. (2) of Ref. [40]. For the 160 Skyrme parametrizations in our Skyrme ensemble, the mean values and covariance matrix of these 10 parameters are presented in Table I. Following the method described in Ref. [78], we employed linear transformations of independent Gaussian random numbers to generate random Skyrme parametrizations that statistically resemble the original set of 160 Skyrme parameters, maintaining similar means, fluctuations, and correlations, as listed in Table I.

Beside the consideration of statistic nature of random Skyrme parameters, we also need to make sure the existence of the nuclear matter governed by such randomized Skyrme force, which may be demonstrated by corresponding saturation density (ρ_0). Unlike 160 Skyrme parametrizations in the Skyrme ensemble, which were well adjusted targeting realistic nuclear properties, the random Skyrme parametrization dose not necessarily provide ρ_0 close to 0.16 fm^{-3} , i.e., the realistic value. The density should be the root of saturation condition equation of

Beyond the statistical nature of random Skyrme parameters, we also ensured the existence of nuclear matter for each randomized Skyrme force by checking for a corresponding saturation density (ρ_0). ρ_0 should be a root of the saturation condition equation:

$$\frac{\hbar^2}{5m} \left(\frac{3\pi^2}{2} \right)^{2/3} \rho_0^{-1/3} + \frac{3}{8}t_0 + \frac{1}{16}t_3(\alpha + 1)\rho_0^\alpha + \frac{1}{16} [3t_1 + t_2(5 + 4x_2)] \left(\frac{3\pi^2}{2} \right)^{2/3} \rho_0^{2/3} = 0. \quad (1)$$

Unlike the 160 Skyrme parametrizations in the Skyrme ensemble which were carefully fitted to reproduce realistic nuclear properties, the random Skyrme parametrizations might not necessarily yield a ρ_0 root close to the realistic value of 0.16 fm^{-3} . In some extreme cases, there might not even be a real positive root, suggesting that nuclear matter might not exist under such a Skyrme force. We considered such parametrizations to be unphysical and therefore excluded them from our ensemble investigation.

We emphasize that this work is aimed at constraining L , which is related to Skyrme parametrization by

$$L = \frac{\hbar^2}{3m} c \rho_0^{2/3} - \frac{3}{8}t_0(1 + 2x_0)\rho_0 - \frac{1}{16}t_3(1 + 2x_3)(\alpha + 1)\rho_0^{\alpha+1} - \frac{5}{24} [3t_1x_1 - t_2(4 + 5x_2)] c \rho_0^{5/3}. \quad (2)$$

To fairly assess the predominance of linear $\Delta R_{\text{np}} - I$ and $\Delta R_{\text{mirr}} - I$ correlations for different L values, and to mitigate potential biases from intrinsic L distribution within the random Skyrme calculations, we sampled approximately 4000 Skyrme parametrizations for each $\Delta L = 5$ MeV interval across the range $L = 0 \sim 200$ MeV. These parametrizations were then used in SHF calculations for the same set of even-even nuclei as in the RQE. Considering that prolate deformation is common in nuclei, we employed an initial single-particle basis with a prolate deformation of $\beta = 0.2$, which likely favors a prolate HF solution. This set of random interaction calculations forms what we denote as the random Skyrme ensemble (RSE) in this paper. For each parametrization within the RSE, we calculated the Pearson’s r for both $\Delta R_{\text{np}} - I$ and $\Delta R_{\text{mirr}} - I$ correlations. We found that

TABLE I. Mean values and covariance matrix of the 160 Skyrme parametrizations in the Skyrme ensemble. The notation of Skyrme parameters follow Eq. (2) of Ref. [40].

	$\langle t_0 \rangle$	$\langle t_1 \rangle$	$\langle t_2 \rangle$	$\langle t_3 \rangle$	$\langle x_0 \rangle$	$\langle x_1 \rangle$	$\langle x_2 \rangle$	$\langle x_3 \rangle$	$\langle W_0 \rangle$	$\langle 1/\sigma \rangle$
mean	-2.03×10^3	394	-156	1.3×10^4	0.443	-0.461	0.471	0.594	134	4.11
covariance	t_0	t_1	t_2	t_3	x_0	x_1	x_2	x_3	W_0	$1/\sigma$
t_0	2.39×10^9	-1.21×10^4	4.26×10^4	-5.39×10^5	-29.5	18.6	247	-86.3	-2.95×10^3	-821
t_1	-1.21×10^4	1.32×10^4	276	-1.52×10^5	0.6	-12.3	-33.1	14	1.21×10^3	65.2
t_2	4.26×10^4	276	1.41×10^5	-2.56×10^5	-77.8	-229	119	-124	4.97×10^3	-140
t_3	-5.39×10^5	-1.52×10^5	-2.56×10^5	8.35×10^6	157	373	-1.22×10^3	49.8	-1.54×10^4	1.49×10^3
x_0	-29.5	0.6	-77.8	157	0.146	0.0574	-0.114	0.241	-0.399	0.134
x_1	18.6	-12.3	-229	373	0.0574	0.688	-0.046	5.04×10^{-3}	-17.9	-0.12
x_2	247	-33.1	119	-1.22×10^3	-0.114	-0.046	46	-0.176	-7.23	-1.01
x_3	-86.3	14	-124	49.8	0.241	5.04×10^{-3}	-0.176	0.484	4.04	0.375
W_0	-2.95×10^3	1.21×10^3	4.97×10^3	-1.54×10^4	-0.399	-17.9	-7.23	4.04	1.82×10^3	13.2
$1/\sigma$	-821	65.2	-140	1.49×10^3	0.134	-0.12	-1.01	0.375	13.2	2.99

there is a 50.6(9)% probability of achieving strong linearity ($r > 0.95$) for $\Delta R_{\text{np}} - I$ and a higher probability of 89(1)% for $\Delta R_{\text{mirr}} - I$. These notably high probabilities are even more significant than those from our RQE calculations. For comparison, we have also included these percentages in Fig. 2. The larger model space in the SHF calculations does indeed appear to strengthen the predominance of linear $\Delta R_{\text{np}} - I$ and $\Delta R_{\text{mirr}} - I$ correlations.

For realistic nuclear systems, nucleons move within an effectively infinite Hilbert space. Based on our observations in Fig. 2, robust linear correlations of $\Delta R_{\text{np}} - I$ and $\Delta R_{\text{mirr}} - I$ are reasonably expected, consistent with experimental findings as shown in Fig. 1.

III. $C_{\text{np}} - L$ AND $C_{\text{mirr}} - L$ LINEARITY

Having presented evidence for the robust linear correlations of $\Delta R_{\text{np}} - I$ and $\Delta R_{\text{mirr}} - I$, we also remind the reported linear relationship between ΔR_{np} (or ΔR_{mirr}) and the symmetry energy slope L [31–36, 38–40]. Given the transitive nature of linearity, one might expect L to also exhibit a linear correlation with I or with the slopes of the $\Delta R_{\text{np}} - I$ and $\Delta R_{\text{mirr}} - I$ correlations (denoted as C_{np} and C_{mirr} , respectively). Since L is understood to be an observable reflecting a bulk property of nuclear matter, and thus independent of specific nucleon numbers like N and Z (i.e., I), we anticipate observing linearity primarily in the $C_{\text{np}} - L$ and $C_{\text{mirr}} - L$ correlations. Therefore, exploring these potential linear relationships seems worthwhile. If such linear correlations are indeed present, and given that C_{np} and C_{mirr} might be experimentally accessible, this could provide a potentially new avenue for constraining the value of L .

A. verification

We now investigate the linearity of the $C_{\text{np}} - L$ and $C_{\text{mirr}} - L$ correlations within the Skyrme ensemble, which

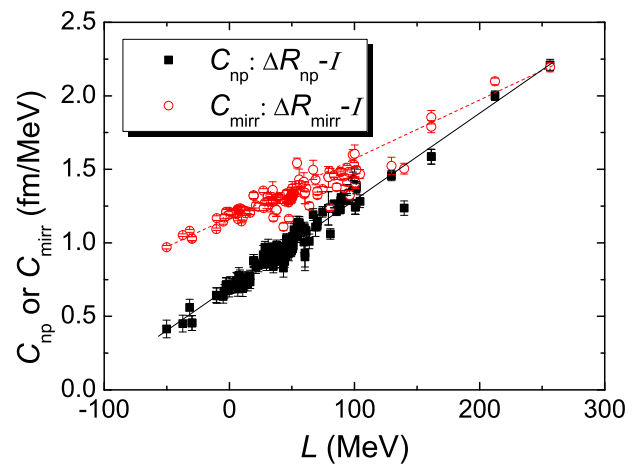


FIG. 3. (Color online) C_{np} and C_{mirr} (slopes of the $\Delta R_{\text{np}} - I$ and $\Delta R_{\text{mirr}} - I$ linear correlations, respectively) as a function of L in the Skyrme ensemble, which includes 160 previously proposed Skyrme parametrizations. The approximate linear trends for both $C_{\text{np}} - L$ and $C_{\text{mirr}} - L$ correlations are visually apparent, highlighted by the black solid and red dashed lines as visual guides.

comprises 160 existing Skyrme parametrizations. As demonstrated previously, all these Skyrme parametrizations yield Pearson's r values greater than 0.85 for both $\Delta R_{\text{np}} - I$ and $\Delta R_{\text{mirr}} - I$ correlations, suggesting that deviations from linear fits for these correlations should be reasonably small. Therefore, we proceed to perform linear fitting for the $\Delta R_{\text{np}} - I$ correlation and proportional fitting for $\Delta R_{\text{mirr}} - I$ correlation. For the proportional fitting of $\Delta R_{\text{mirr}} - I$, we omit the intercept, recognizing that $\Delta R_{\text{mirr}} \equiv 0$ at $I = 0$. Figure 3 then displays the plots of the extracted slopes, C_{np} and C_{mirr} , as a function of L for each parametrization in the Skyrme ensemble. These plots indicate a general linear trend for both $C_{\text{np}} - L$ and $C_{\text{mirr}} - L$ correlations. It is also worth noting that for lower L values (< 100 MeV), C_{np} tends to be systematically smaller than C_{mirr} , while the difference between C_{np} and C_{mirr} gradually diminishes as L

increases.

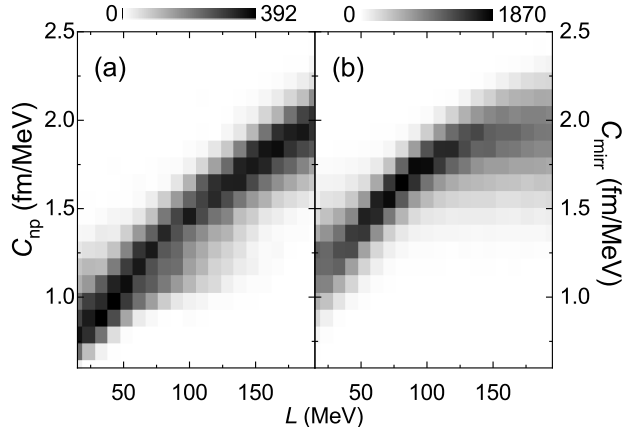


FIG. 4. Grey scale maps illustrating the two-dimensional counting of $\{C_{\text{np}}, L\}$ and $\{C_{\text{mirr}}, L\}$ data pairs from the RSE. Only C_{np} and C_{mirr} values with corresponding Pearson's r greater than 0.85 are included. Panel (a) shows a clear linear correlation between C_{np} and L , consistent with Fig. 3. Panel (b) presents the correlation between C_{mirr} and L . Unlike the $C_{\text{np}} - L$ correlation, the linear trend in the $C_{\text{mirr}} - L$ correlation appears to weaken at larger L values.

We also observe the linear correlation between C_{np} and L , and between C_{mirr} and L in the RSE. For Skyrme parametrizations in the RSE that exhibit Pearson's r values above 0.85, we perform two-dimensional counting of $\{C_{\text{np}}, L\}$ and $\{C_{\text{mirr}}, L\}$ data pairs. The results are shown in Fig. 4 using gray scale mapping. As shown in Fig. 4(a), a linear correlation between C_{np} and L is apparent. However, as depicted in Fig. 4(b), the linear correlation of $C_{\text{mirr}} - L$ seems to be maintained primarily for $L < 150$ MeV. Beyond $L = 150$ MeV, the slope of this correlation appears to decrease. Consistent with observations from the Skyrme ensemble using well-established Skyrme parametrizations, for lower L values (< 100 MeV), C_{np} tends to be systematically smaller than C_{mirr} , whereas at higher L values, they become quantitatively comparable.

B. explanation

To understand the possible origin of the robust linear correlations observed for $C_{\text{np}} - L$ and $C_{\text{mirr}} - L$, we focus on $C_{\text{np}} - L$, assuming that the robust linearity of $C_{\text{mirr}} - L$ reflects a similar underlying mechanism. Following the formalism from the supplement of Ref. [44], we have:

$$C_{\text{np}} = \frac{3}{2} r_0 \frac{J}{Q^*}, \quad (3)$$

where J is the symmetry energy coefficient, r_0 is the oscillation parameter, and Q^* represents the effective surface stiffness coefficient, which describes the resistance to the pulling apart of neutrons and protons at the nuclear surface. Both J and L are functions of the Skyrme

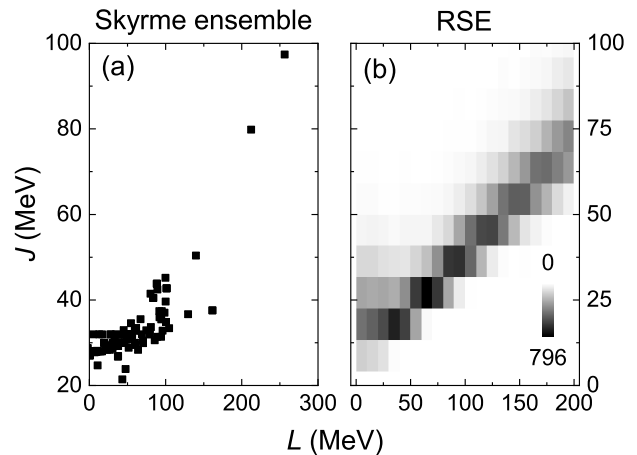


FIG. 5. J against L in the Skyrme ensemble and RSE ensemble, as shown in Panel (a) and (b) respectively. Panel (b) shows a two-dimensional counting for $\{J, L\}$ combinations.

parametrization. Furthermore, it's worth noting that Q^* is related to specific N and Z values within many-body calculations (as in Ref. [79]). Given that the linear correlation of $\Delta R_{\text{np}} - L$ is observed to be robust across the nuclear chart, one might expect C_{np} to be relatively stable with respect to variations in N and Z . This would further suggest that the N and Z dependence of Q^* may not significantly impact C_{np} . Therefore, for simplicity and following the approach of Ref. [44], we can consider Q^* to be approximately constant compared to the variation of J . Consequently, if C_{np} and L are linearly correlated, Eq. (3) implies a corresponding linear correlation between J and L within the L range where we observe the $C_{\text{np}} - L$ linearity, as shown in Figs. 3 and 4(a). To examine the linearity of the $J - L$ correlation, we plot J , calculated using

$$J = \frac{\hbar^2}{6m} c \rho^{2/3} - \frac{1}{8} t_0 (1 + 2x_0) \rho - \frac{1}{48} t_3 (1 + 2x_3) \rho^{\alpha+1} - \frac{1}{24} [3t_1 x_1 - t_2 (4 + 5x_2)] c \rho^{5/3} \quad (4)$$

against L , calculated using Eq. (2), for each of the 160 parametrizations in the Skyrme ensemble in Fig. 5(a). While some fluctuation in the $J - L$ correlation is present for $L < 50$ MeV, a roughly linear trend appears to emerge in the range $L = 50 \sim 300$ MeV. In the RSE, we repeated similar calculations and present the $\{J, L\}$ pairs as a two-dimensional histogram in Fig. 5(b). The linearity of $J - L$ becomes more evident, which may offer a possible explanation for the robust linear $C_{\text{np}} - L$ correlation.

We now consider why L and J exhibit a linear correlation. Let us rewrite J from Eq. (4) as a sum of four

terms:

$$\begin{aligned}
 J &= J_1 + J_2 + J_3 + J_4 \\
 J_1 &= \frac{\hbar^2}{6m} c\rho^{2/3} \\
 J_2 &= -\frac{1}{8}t_0(1 + 2x_0)\rho \\
 J_3 &= -\frac{1}{48}t_3(1 + 2x_3)\rho^{\alpha+1} \\
 J_4 &= -\frac{1}{24}[3t_1x_1 - t_2(4 + 5x_2)]c\rho^{5/3}.
 \end{aligned} \tag{5}$$

Correspondingly, we can also express L from Eq. (2) in terms of J_1 , J_2 , J_3 , and J_4 as:

$$L = 2J_1 + 3J_2 + 4(1 + \sigma)J_3 + 5J_4. \tag{6}$$

We observe that both L and J are linear combinations of J_1 , J_2 , J_3 , and J_4 . In a numerical test, assuming J_1 , J_2 , J_3 , J_4 , and σ are independent random numbers following a normal distribution, we found that the probability of obtaining a Pearson's $r > 0.9$ for ten $\{J, L\}$ data pairs, calculated using Eqs. (5) and (6), is approximately 49(2)%. In contrast, if ten $\{J, L\}$ data pairs are independently sampled from normal distributions, this probability is only around 1.90(4)%. The similarity in the linear combination structure for J and L as shown in Eqs. (5) and (6) likely enhances the linear correlation between them, and consequently, the linearity between L and C_{np} . This formulation similarity may offer a partial explanation for the observed robust linear correlations in Figs. 3 and 4.

IV. L CONSTRAINT

A. C_{np} and C_{mirr} constraint

We further emphasize that the linear correlations of $C_{\text{np}} - L$ and $C_{\text{mirr}} - L$ are not only novel, but also potentially valuable for constraining L . First, experimental data in Fig. 1 indicates that C_{np} is smaller than C_{mirr} . This suggests a possible upper limit for L around 100 MeV, as they appear to become comparable at $L = 100$ MeV, as shown in Fig. 3. This observation may be crucial, especially considering that $L \approx 100$ MeV is often discussed as a boundary between soft and stiff EOS [39, 80]. Second, the robust linearity of the $C_{\text{np}} - L$ and $C_{\text{mirr}} - L$ correlations, along with their considerable slopes, makes C_{np} and C_{mirr} sensitive indicators of L , potentially enabling constraints with smaller uncertainty. Third, C_{np} and C_{mirr} are comprehensive observables, since they incorporate information from all experimental R_{np} and R_{mirr} data. Consequently, L constraints from these observables could largely mitigate the interference from density anomalies in specific nuclei with exotic structures.

More precisely, we sample the Skyrme parametrizations in the RSE, which could reproduce the linearity of

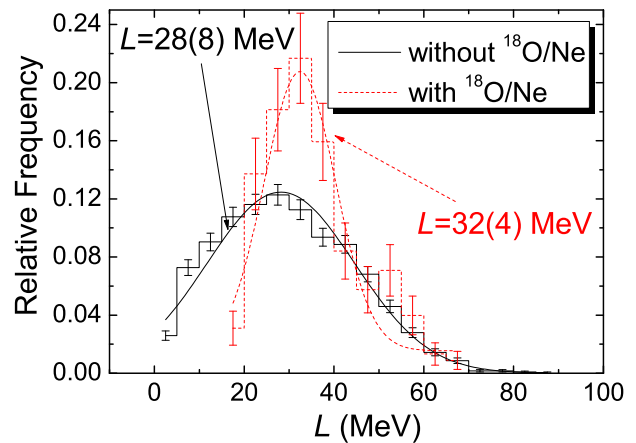


FIG. 6. (Color online) Distributions of the symmetry energy slope parameter L for two subsets of Skyrme parametrizations within the RSE. The black solid histograms correspond to parametrizations that reproduce the linearity of $\Delta R_{\text{np}} - I$ and $\Delta R_{\text{mirr}} - I$ with Pearson's $r > 0.85$ and 0.99 , respectively, and yield corresponding C_{np} and C_{mirr} values within experimental uncertainties. The red dashed histograms correspond to those parametrizations that additionally reproduce ΔR_{mirr} for the $^{18}\text{O}/\text{Ne}$ mirror pair within experimental uncertainties, considering the potential shape coexistence of ^{18}O . Step histograms are from sample counts, with error bars representing statistical uncertainties. The curves represent Gaussian fits, providing constraints on $L = 28 \pm 8$ MeV and 32 ± 4 MeV with and without including the ΔR_{mirr} data for the $^{18}\text{O}/\text{Ne}$ mirror pair, respectively.

$\Delta R_{\text{np}} - I$ and $\Delta R_{\text{mirr}} - I$ with Pearson's $r > 0.85$ and 0.99 respectively, and corresponding C_{np} and C_{mirr} within experimental error. Approximately 2000 parametrizations met these sampling criteria. The L distribution of these sampled parametrization demonstrate the reasonable range of L . In Fig. 6, the black solid step line presents such a distribution. The distribution brings a peak, which can be fitted by an Gaussian function. The fitting curve is presented in Fig. 6 with black solid line with peak center at 28.2 and width 16.4. Thus, according to the experimental slope of $\Delta R_{\text{np}} - I$ and $\Delta R_{\text{mirr}} - I$, $L = 28_{-8}^{+8}$ MeV with 1σ confidence.

To perform this constraint, we sampled Skyrme parametrizations from the RSE that could reproduce the linearity of $\Delta R_{\text{np}} - I$ and $\Delta R_{\text{mirr}} - I$ (Pearson's $r > 0.85$ and 0.99 , respectively), and yield C_{np} and C_{mirr} values consistent with experimental $C_{\text{np}} = 0.9(1)$ fm/MeV and $C_{\text{mirr}} = 1.31(4)$ fm/MeV from Fig. 1. The L distribution of these sampled parametrizations demonstrates a plausible range for L . In Fig. 6, the black solid step histogram represents this distribution. The distribution exhibits a peak, which is well described by a Gaussian function. The Gaussian fit is shown as a black solid curve in Fig. 6, with a peak center at 28 MeV and a width of 16 MeV. Therefore, based on the slopes of experimental $\Delta R_{\text{np}} - I$ and $\Delta R_{\text{mirr}} - I$ correlation, we estimate $L = 28 \pm 8$ MeV at the 1σ confidence level.

B. shape effect on ΔR_{mirr} deviations

Given the robust linearity of the $\Delta R_{\text{mirr}} - I$ correlation, and the clear deviation of experimental ΔR_{mirr} for $^{18}\text{O}/\text{Ne}$ from this linear trend, we expect that Skyrme parametrizations reproducing the experimental linear $\Delta R_{\text{mirr}} - I$ behavior would likely fail to reproduce the experimental ΔR_{np} of $^{18}\text{O}/\text{Ne}$. To verify this, we make an attempt to select Skyrme parametrizations that could simultaneously reproduce the linear $\Delta R_{\text{np}} - I$ and $\Delta R_{\text{mirr}} - I$ correlations with experimental slopes, and the experimental ΔR_{np} of $^{18}\text{O}/\text{Ne}$ within a 1σ confidence interval. Among approximately 150,000 parametrizations in the RSE, we found none that met these selection criteria. This suggests a significant discrepancy between $^{18}\text{O}/\text{Ne}$ and other even-even nuclei regarding the $\Delta R_{\text{mirr}} - I$ linearity. More importantly, this discrepancy appears to prevent us from finding suitable Skyrme parametrizations, and consequently reasonable constraints on L , capable of reproducing all experimental ΔR_{np} and ΔR_{mirr} data for even-even nuclei. This outcome is not satisfactory.

To address this apparent discrepancy and to obtain an L constraint that is consistent with the $^{18}\text{O}/\text{Ne}$ ΔR_{mirr} data, it seems necessary to explain the deviation of the $^{18}\text{O}/\text{Ne}$ mirror pair observed in Fig. 1. We recall that ^{18}O and ^{18}Ne are both candidates for shape coexistence [81]. Recent studies also indicate that shape coexistence might be a widespread phenomenon across the nuclide chart [82]. Different nuclear shapes could naturally lead to different charge radii. Thus, it is conceivable that shape coexistence in the $^{18}\text{O}/\text{Ne}$ pair results in multiple ΔR_{mirr} values. One of these values might follow the general linear trend of $\Delta R_{\text{mirr}} - I$, potentially originating from one or two local minima in the Hartree-Fock potential energy surface of $^{18}\text{O}/\text{Ne}$. Another ΔR_{mirr} value might then agree with the experimental ΔR_{mirr} of $^{18}\text{O}/\text{Ne}$, corresponding to Hartree-Fock ground states. However, as mentioned earlier, our initial SHF calculations started from a basis with $\beta = 0.2$, which may primarily converge to a single prolate deformation and thus potentially hinder the consistent reproduction of both the linear $\Delta R_{\text{mirr}} - I$ correlation and the specific ΔR_{mirr} of $^{18}\text{O}/\text{Ne}$.

To further explore this shape coexistence picture, we repeated the SHF calculations for $^{18}\text{O}/\text{Ne}$ with the ~ 2000 parametrizations sampled from the RSE, which could reproduce the experimental linear correlations of $\Delta R_{\text{np}} - I$ and $\Delta R_{\text{mirr}} - I$, as described in Sec. IV A. To allow for the possibility of shape coexistence, these calculations started from a single-particle basis with $\beta = -0.2 \sim 0.2$ with 0.01 interval, where negative β values indicate oblate shapes. As expected, for each parametrization, the SHF calculations may yield several ΔR_{mirr} values for $^{18}\text{O}/\text{Ne}$. Given the robust $\Delta R_{\text{mirr}} - I$ linearity, we anticipated that one of these values would align with the experimental $\Delta R_{\text{mirr}} - I$ trend. Notably, among these ~ 2000 parametrizations, approximately 200 also pro-

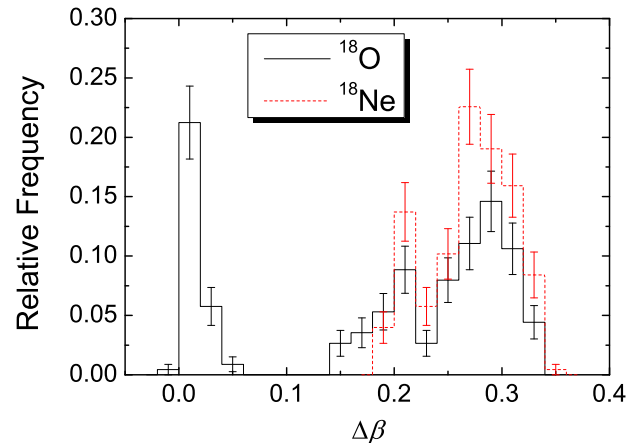


FIG. 7. (Color online) Distributions of β differences ($\Delta\beta$) for ^{18}O and ^{18}Ne between two shapes, obtained from RSE parametrizations that reproduce both the experimental $\Delta R_{\text{mirr}} - I$ linearity and the experimental ΔR_{mirr} of $^{18}\text{O}/\text{Ne}$ (within 1σ confidence). Non-zero $\Delta\beta$ values are indicative of shape coexistence.

duced a ΔR_{mirr} value consistent with experimental data for $^{18}\text{O}/\text{Ne}$. Thus, these ~ 200 parametrizations yielded at least two ΔR_{mirr} values, presumably originating from different shapes of ^{18}O and/or ^{18}Ne . To illustrate the shape difference, we calculated the β differences ($\Delta\beta$) of ^{18}O and ^{18}Ne between two shapes, one that produces ΔR_{mirr} following the experimental $\Delta R_{\text{mirr}} - I$ linearity, and the other that reproduces the experimental ΔR_{mirr} of $^{18}\text{O}/\text{Ne}$, within 1σ confidence. The distribution of these $\Delta\beta$ values from these ~ 200 parametrizations is shown in Fig. 7. For ^{18}O , we observe three peaks in the distribution, around $\Delta\beta \sim 0, 0.2$, and 0.3 . These peaks may correspond to scenarios of no shape coexistence, spherical-deformed coexistence (between $\beta \simeq 0$ and ± 0.2), and prolate-oblate coexistence (between $\beta \simeq 0.2$ and -0.1 , or $\beta \simeq 0.1$ and -0.2). For ^{18}Ne , two peaks are located at $\Delta\beta \sim 0.2$ and 0.3 , similarly hinting at spherical-deformed and prolate-oblate coexistence. Therefore, to reasonably reproduce the linear $\Delta R_{\text{np}} - I$ and $\Delta R_{\text{mirr}} - I$ correlations, along with the ΔR_{mirr} of $^{18}\text{O}/\text{Ne}$ using a single Skyrme parametrization, incorporating shape coexistence, at least for ^{18}Ne , appears to be necessary. Shape coexistence in ^{18}O may also be occasionally required.

Finally, using the ~ 200 Skyrme parametrizations sampled above, considering the experimental ΔR_{mirr} fit for $^{18}\text{O}/\text{Ne}$, we can also estimate another constraint on L . The distribution of L values for these parametrizations is plotted in Fig. 6. A Gaussian fit to this distribution suggests a value of $L = 32(4)$ MeV within the 1σ confidence.

Given the considerable influence of nuclear shape on the $\Delta R_{\text{mirr}} - I$ linearity, we propose that it may also contribute to the less systematic behavior observed for odd- A ΔR_{mirr} values. For doubly-even mirror pair, ΔR_{mirr} corresponds to a charge-radius difference between two

even-like-nucleon systems, while for odd- A pair, it corresponds to difference between odd-like-nucleon system and even-like-nucleon system. The shapes of even-like-nucleon systems are typically governed by nuclear collectivity, and are generally stable within a local isotopic region. However, the deformation of odd-like-nucleon systems can be significantly influenced by the unpaired single nucleon. The specific orbit occupied by this unpaired nucleon can introduce discontinuities in nuclear structure, potentially leading to discontinuous shape evolution. This distinction between even and odd systems is also reflected in phenomena such as the shape staggering observed in charge radii of Hg and Cu isotopes [83, 84]. Based on this reasoning, ΔR_{mirr} for even-even nuclei primarily reflects the difference in collectivity between two even-like-nucleon systems, which may follow a continuous local trend, and captures the general regularity of finite nuclear matter, i.e., the $\Delta R_{\text{mirr}} - I$ linearity. In contrast, for odd- A nuclei, the discontinuities introduced by the unpaired nucleon can lead to a more scattered, or less systematically organized, ΔR_{mirr} behavior. Thus, odd- A ΔR_{mirr} values may exhibit larger deviations from the $\Delta R_{\text{mirr}} - I$ linearity compared to even-even nuclei.

V. SUMMARY

In summary, we have observed various linear correlations related to neutron skin thickness (ΔR_{np}) in random interaction ensembles. These include random quasiparticle ensemble (RQE) with shell model calculation, and the newly proposed random Skyrme ensemble (RSE) with Hatree-Fock calculations, as well as the Skyrme ensemble based on 160 previously proposed and physically-

tuned Skyrme parametrizations. The RSE is designed to align with the statistical properties (means and covariance matrix) of the Skyrme ensemble.

The linear correlation between ΔR_{np} , or charge radius difference of mirror nuclei (ΔR_{mirr}), and the isospin asymmetry ($I = \frac{N-Z}{A}$) become more obvious in the random interaction, as increasing model space. In the Skyrme ensemble, this linear correlation is reproduced by all Skyrme parametrizations. The robustness of this linear correlation suggests that it reflects a nature of finite nuclear matter.

In Sec. IV B, we have further explain the obvious deviation of $^{18}\text{O}/\text{Ne}$ ΔR_{mirr} from the $\Delta R_{\text{mirr}} - I$ linearity, considering that ^{18}O and ^{18}Ne are both candidates for shape coexistence. Following a similar line of reasoning, we also attribute the less systematic behavior of ΔR_{mirr} in odd- A mirror nuclei to the shape variations arising from the single-particle motion of the unpaired nucleon.

Within the Skyrme ensemble, and the RSE, the slopes of the linear $\Delta R_{\text{np}} - I$ and $\Delta R_{\text{mirr}} - I$ correlations (C_{np} and C_{mirr} , respectively) are also robustly and linearly correlated to the slope of the symmetry energy (L) against nucleon density at equilibrium density in the nuclear equation of state. This correlation is further explained with the similar formulation between between L and the symmetry energy coefficient (J), as described by Eqs. (5) and (6).

The linear $C_{\text{np}} - L$ and $C_{\text{mirr}} - L$ correlations have been used to constrain L to $20 \sim 36$ MeV, based on the sampling in the RSE. Considering the deviation of $^{18}\text{O}/\text{Ne}$ ΔR_{mirr} , the 1σ range of L is further reduced to $28 \sim 36$ MeV, tentatively suggesting a relatively soft EOS.

-
- [1] J. M. Lattimer and M. Prakash, Neutron star observations: Prognosis for equation of state constraints, *Physics Reports* **442**, 109 (2007), the Hans Bethe Centennial Volume 1906-2006.
 - [2] M. Oertel, M. Hempel, T. Klähn, and S. Typel, Equations of state for supernovae and compact stars, *Rev. Mod. Phys.* **89**, 015007 (2017).
 - [3] B. Alex Brown, Neutron radii in nuclei and the neutron equation of state, *Phys. Rev. Lett.* **85**, 5296 (2000).
 - [4] S. Typel and B. A. Brown, Neutron radii and the neutron equation of state in relativistic models, *Phys. Rev. C* **64**, 027302 (2001).
 - [5] R. Furnstahl, Neutron radii in mean-field models, *Nuclear Physics A* **706**, 85 (2002).
 - [6] A. Steiner, M. Prakash, J. Lattimer, and P. Ellis, Isospin asymmetry in nuclei and neutron stars, *Physics Reports* **411**, 325 (2005).
 - [7] B. G. Todd-Rutel and J. Piekarewicz, Neutron-rich nuclei and neutron stars: A new accurately calibrated interaction for the study of neutron-rich matter, *Phys. Rev. Lett.* **95**, 122501 (2005).
 - [8] M. Centelles, X. Roca-Maza, X. Viñas, and M. Warda, Nuclear symmetry energy probed by neutron skin thickness of nuclei, *Phys. Rev. Lett.* **102**, 122502 (2009).
 - [9] M. Warda, X. Viñas, X. Roca-Maza, and M. Centelles, Neutron skin thickness in the droplet model with surface width dependence: Indications of softness of the nuclear symmetry energy, *Phys. Rev. C* **80**, 024316 (2009).
 - [10] A. Carbone, G. Colò, A. Bracco, L.-G. Cao, P. F. Bortignon, F. Camera, and O. Wieland, Constraints on the symmetry energy and neutron skins from pygmy resonances in ^{68}Ni and ^{132}Sn , *Phys. Rev. C* **81**, 041301 (2010).
 - [11] L.-W. Chen, C. M. Ko, B.-A. Li, and J. Xu, Density slope of the nuclear symmetry energy from the neutron skin thickness of heavy nuclei, *Phys. Rev. C* **82**, 024321 (2010).
 - [12] B. Alex Brown, Neutron radii in nuclei and the neutron equation of state, *Phys. Rev. Lett.* **85**, 5296 (2000).
 - [13] C. J. Horowitz and J. Piekarewicz, Neutron star structure and the neutron radius of ^{208}pb , *Phys. Rev. Lett.* **86**, 5647 (2001).
 - [14] M. B. Tsang, J. R. Stone, F. Camera, P. Danielewicz, S. Gandolfi, K. Hebeler, C. J. Horowitz, J. Lee, W. G.

- Lynch, Z. Kohley, R. Lemmon, P. Möller, T. Murakami, S. Riordan, X. Roca-Maza, F. Sammarruca, A. W. Steiner, I. Vidaña, and S. J. Yennello, Constraints on the symmetry energy and neutron skins from experiments and theory, *Phys. Rev. C* **86**, 015803 (2012).
- [15] G. Hagen, A. Ekström, C. Forssén, G. R. Jansen, W. Nazarewicz, T. Papenbrock, K. A. Wendt, S. Bacca, N. Barnea, B. Carlsson, C. Drischler, K. Hebeler, M. Hjorth-Jensen, M. Miorelli, G. Orlandini, A. Schwenk, and J. Simonis, Neutron and weak-charge distributions of the ^{48}Ca nucleus, *Nature Physics* **12**, 186 (2016).
- [16] B. A. Brown, Mirror charge radii and the neutron equation of state, *Phys. Rev. Lett.* **119**, 122502 (2017).
- [17] F. J. Fattoyev, J. Piekarewicz, and C. J. Horowitz, Neutron skins and neutron stars in the multimessenger era, *Phys. Rev. Lett.* **120**, 172702 (2018).
- [18] C. A. Bertulani and J. Valencia, Neutron skins as laboratory constraints on properties of neutron stars and on what we can learn from heavy ion fragmentation reactions, *Phys. Rev. C* **100**, 015802 (2019).
- [19] X. Roca-Maza, M. Centelles, X. Viñas, and M. Warda, Neutron skin of ^{208}Pb , nuclear symmetry energy, and the parity radius experiment, *Phys. Rev. Lett.* **106**, 252501 (2011).
- [20] P.-G. Reinhard and W. Nazarewicz, Nuclear charge and neutron radii and nuclear matter: Trend analysis in skyrme density-functional-theory approach, *Phys. Rev. C* **93**, 051303 (2016).
- [21] A. Steiner, M. Prakash, J. Lattimer, and P. Ellis, Isospin asymmetry in nuclei and neutron stars, *Physics Reports* **411**, 325 (2005).
- [22] B. Alex Brown, Neutron radii in nuclei and the neutron equation of state, *Phys. Rev. Lett.* **85**, 5296 (2000).
- [23] B. A. Brown, Mirror charge radii and the neutron equation of state, *Phys. Rev. Lett.* **119**, 122502 (2017).
- [24] L.-W. Chen, C. M. Ko, and B.-A. Li, Nuclear matter symmetry energy and the neutron skin thickness of heavy nuclei, *Phys. Rev. C* **72**, 064309 (2005).
- [25] B.-A. Li and X. Han, Constraining the neutron-proton effective mass splitting using empirical constraints on the density dependence of nuclear symmetry energy around normal density, *Physics Letters B* **727**, 276 (2013).
- [26] M. Oertel, M. Hempel, T. Klähn, and S. Typel, Equations of state for supernovae and compact stars, *Rev. Mod. Phys.* **89**, 015007 (2017).
- [27] C. Drischler, R. J. Furnstahl, J. A. Melendez, and D. R. Phillips, How well do we know the neutron-matter equation of state at the densities inside neutron stars? a bayesian approach with correlated uncertainties, *Phys. Rev. Lett.* **125**, 202702 (2020).
- [28] B.-A. Li, B.-J. Cai, W.-J. Xie, and N.-B. Zhang, Progress in constraining nuclear symmetry energy using neutron star observables since gw170817, *Universe* **7**, 10.3390/universe7060182 (2021).
- [29] A. Carbone, G. Colò, A. Bracco, L.-G. Cao, P. F. Bortignon, F. Camera, and O. Wieland, Constraints on the symmetry energy and neutron skins from pygmy resonances in ^{68}Ni and ^{132}Sn , *Phys. Rev. C* **81**, 041301 (2010).
- [30] X. Roca-Maza, M. Brenna, B. K. Agrawal, P. F. Bortignon, G. Colò, L.-G. Cao, N. Paar, and D. Vretenar, Giant quadrupole resonances in ^{208}pb , the nuclear symmetry energy, and the neutron skin thickness, *Phys. Rev. C* **87**, 034301 (2013).
- [31] Z. Zhang and L.-W. Chen, Constraining the symmetry energy at subsaturation densities using isotope binding energy difference and neutron skin thickness, *Physics Letters B* **726**, 234 (2013).
- [32] C. Mondal, B. K. Agrawal, M. Centelles, G. Colò, X. Roca-Maza, N. Paar, X. Viñas, S. K. Singh, and S. K. Patra, Model dependence of the neutron-skin thickness on the symmetry energy, *Phys. Rev. C* **93**, 064303 (2016).
- [33] L. Min, L. Zhu-Xia, W. Ning, and Z. Feng-Shou, Exploring nuclear symmetry energy with isospin dependence in neutron skin thickness of nuclei, *Chinese Physics C* **35**, 629 (2011).
- [34] X. Fan, J. Dong, and W. Zuo, Symmetry energy at subsaturation densities and the neutron skin thickness of ^{208}pb , *Science China Physics, Mechanics & Astronomy* **58**, 1 (2015).
- [35] C. Xu, Z. Ren, and J. Liu, Attempt to link the neutron skin thickness of ^{208}Pb with the symmetry energy through cluster radioactivity, *Phys. Rev. C* **90**, 064310 (2014).
- [36] J. Xu, W.-J. Xie, and B.-A. Li, Bayesian inference of nuclear symmetry energy from measured and imagined neutron skin thickness in $^{116,118,120,122,124,130,132}\text{Sn}$, ^{208}Pb , and ^{48}Ca , *Phys. Rev. C* **102**, 044316 (2020).
- [37] N. Wang and T. Li, Shell and isospin effects in nuclear charge radii, *Phys. Rev. C* **88**, 011301 (2013).
- [38] B. A. Brown, K. Minamisono, J. Piekarewicz, H. Hergert, D. Garand, A. Klose, K. König, J. D. Lantis, Y. Liu, B. Maaß, A. J. Miller, W. Nörtershäuser, S. V. Pineda, R. C. Powel, D. M. Rossi, F. Sommer, C. Sumithrarachchi, A. Teigelhöfer, J. Watkins, and R. Wirth, Implications of the $^{36}\text{Ca}-^{36}\text{S}$ and $^{38}\text{Ca}-^{38}\text{Ar}$ difference in mirror charge radii on the neutron matter equation of state, *Phys. Rev. Res.* **2**, 022035 (2020).
- [39] S. V. Pineda, K. König, D. M. Rossi, B. A. Brown, A. Incorvati, J. Lantis, K. Minamisono, W. Nörtershäuser, J. Piekarewicz, R. Powel, and F. Sommer, Charge radius of neutron-deficient ^{54}Ni and symmetry energy constraints using the difference in mirror pair charge radii, *Phys. Rev. Lett.* **127**, 182503 (2021).
- [40] R. An, S. Sun, L.-G. Cao, and F.-S. Zhang, Constraining nuclear symmetry energy with the charge radii of mirror-pair nuclei, *Nuclear Science and Techniques* **34**, 119 (2023).
- [41] Y. N. Huang, Z. Z. Li, and Y. F. Niu, Correlation between the difference of charge radii in mirror nuclei and the slope parameter of the symmetry energy, *Phys. Rev. C* **107**, 034319 (2023).
- [42] T. Li, Y. Luo, and N. Wang, Compilation of recent nuclear ground state charge radius measurements and tests for models, *Atomic Data and Nuclear Data Tables* **140**, 101440 (2021).
- [43] A. Trzcíńska, J. Jastrzębski, P. Lubiński, F. J. Hartmann, R. Schmidt, T. von Egidy, and B. Kłos, Neutron density distributions deduced from antiprotonic atoms, *Phys. Rev. Lett.* **87**, 082501 (2001).
- [44] S. J. Novario, D. Lonardonì, S. Gandolfi, and G. Hagen, Trends of neutron skins and radii of mirror nuclei from first principles, *Phys. Rev. Lett.* **130**, 032501 (2023).
- [45] W. D. Myers and W. Swiatecki, Average nuclear properties, *Annals of Physics* **55**, 395 (1969).
- [46] W. Myers and W. Swiatecki, The nuclear droplet model for arbitrary shapes, *Annals of Physics* **84**, 186 (1974).
- [47] W. Myers and W. Swiatecki, Droplet-model theory of the

- neutron skin, *Nuclear Physics A* **336**, 267 (1980).
- [48] C. Pethick and D. Ravenhall, The dependence of neutron skin thickness and surface tension on neutron excess, *Nuclear Physics A* **606**, 173 (1996).
- [49] J. Zenihiro, H. Sakaguchi, S. Terashima, T. Uesaka, G. Hagen, M. Itoh, T. Murakami, Y. Nakatsugawa, T. Ohnishi, H. Sagawa, H. Takeda, M. Uchida, H. P. Yoshida, S. Yoshida, and M. Yosoi, *Direct determination of the neutron skin thicknesses in $^{40,48}\text{Ca}$ from proton elastic scattering at $e_p = 295$ mev* (2018), [arXiv:1810.11796 \[nucl-ex\]](https://arxiv.org/abs/1810.11796).
- [50] J. JASTRZEBSKI, A. TRZCIŃSKA, P. LUBIŃSKI, B. KLOS, F. J. HARTMANN, T. von EGIDY, and S. WYCECH, Neutron density distributions from antiprotonic atoms compared with hadron scattering data, *International Journal of Modern Physics E* **13**, 343 (2004), <https://doi.org/10.1142/S0218301304002168>.
- [51] W. R. Gibbs and J.-P. Dedonder, Neutron radii of the calcium isotopes, *Phys. Rev. C* **46**, 1825 (1992).
- [52] D. Adhikari, H. Albatineh, D. Androic, K. A. Aniol, D. S. Armstrong, T. Averett, C. Ayerbe Gayoso, S. K. Barcus, V. Bellini, R. S. Beminiwattha, J. F. Benesch, H. Bhatt, D. Bhatta Pathak, D. Bhetuwal, B. Blaikie, J. Boyd, Q. Campagna, A. Camsonne, G. D. Cates, Y. Chen, C. Clarke, J. C. Cornejo, S. Covrig Dusa, M. M. Dalton, P. Datta, A. Deshpande, D. Dutta, C. Feldman, E. Fuchey, C. Gal, D. Gaskell, T. Gautam, M. Gericke, C. Ghosh, I. Halilovic, J.-O. Hansen, O. Hassan, F. Hauenstein, W. Henry, C. J. Horowitz, C. Jantzi, S. Jian, S. Johnston, D. C. Jones, S. Kakkar, S. Katugampola, C. Keppel, P. M. King, D. E. King, K. S. Kumar, T. Kutz, N. Lashley-Colthirst, G. Leverick, H. Liu, N. Liyanage, J. Mammei, R. Mammei, M. McCaughan, D. McNulty, D. Meekins, C. Metts, R. Michaels, M. Mihovilovic, M. M. Mondal, J. Napolitano, A. Narayan, D. Nikolaev, V. Owen, C. Palatchi, J. Pan, B. Pandey, S. Park, K. D. Paschke, M. Petrusky, M. L. Pitt, S. Premathilake, B. Quinn, R. Radloff, S. Rahman, M. N. H. Rashad, A. Rathnayake, B. T. Reed, P. E. Reimer, R. Richards, S. Riordan, Y. R. Roblin, S. Seeds, A. Shahinyan, P. Souder, M. Thiel, Y. Tian, G. M. Urciuoli, E. W. Wertz, B. Wojtsekhowski, B. Yale, T. Ye, A. Yoon, W. Xiong, A. Zec, W. Zhang, J. Zhang, and X. Zheng (CREX Collaboration), Precision determination of the neutral weak form factor of ^{48}Ca , *Phys. Rev. Lett.* **129**, 042501 (2022).
- [53] G. Giacalone, G. Nijs, and W. van der Schee, Determination of the neutron skin of ^{208}Pb from ultrarelativistic nuclear collisions, *Phys. Rev. Lett.* **131**, 202302 (2023).
- [54] D. Adhikari, H. Albatineh, D. Androic, K. Aniol, D. S. Armstrong, T. Averett, C. Ayerbe Gayoso, S. Barcus, V. Bellini, R. S. Beminiwattha, J. F. Benesch, H. Bhatt, D. Bhatta Pathak, D. Bhetuwal, B. Blaikie, Q. Campagna, A. Camsonne, G. D. Cates, Y. Chen, C. Clarke, J. C. Cornejo, S. Covrig Dusa, P. Datta, A. Deshpande, D. Dutta, C. Feldman, E. Fuchey, C. Gal, D. Gaskell, T. Gautam, M. Gericke, C. Ghosh, I. Halilovic, J.-O. Hansen, F. Hauenstein, W. Henry, C. J. Horowitz, C. Jantzi, S. Jian, S. Johnston, D. C. Jones, B. Karki, S. Katugampola, C. Keppel, P. M. King, D. E. King, M. Knauss, K. S. Kumar, T. Kutz, N. Lashley-Colthirst, G. Leverick, H. Liu, N. Liyanage, S. Malace, R. Mammei, J. Mammei, M. McCaughan, D. McNulty, D. Meekins, C. Metts, R. Michaels, M. M. Mondal, J. Napolitano, A. Narayan, D. Nikolaev, M. N. H. Rashad, V. Owen, C. Palatchi, J. Pan, B. Pandey, S. Park, K. D. Paschke, M. Petrusky, M. L. Pitt, S. Premathilake, A. J. R. Puckett, B. Quinn, R. Radloff, S. Rahman, A. Rathnayake, B. T. Reed, P. E. Reimer, R. Richards, S. Riordan, Y. Roblin, S. Seeds, A. Shahinyan, P. Souder, L. Tang, M. Thiel, Y. Tian, G. M. Urciuoli, E. W. Wertz, B. Wojtsekhowski, B. Yale, T. Ye, A. Yoon, A. Zec, W. Zhang, J. Zhang, and X. Zheng (PREX Collaboration), Accurate determination of the neutron skin thickness of ^{208}Pb through parity-violation in electron scattering, *Phys. Rev. Lett.* **126**, 172502 (2021).
- [55] A. Alexandrovich, A. Gagarski, I. Krasnoschekova, G. Petrov, V. Petrova, A. Petukhov, Y. Pleva, P. Geltenbort, J. Last, and K. Schreckenbach, New observation of space-parity violation in neutron-induced fission of ^{229}Th , ^{241}Pu and ^{241}Am , *Nuclear Physics A* **567**, 541 (1994).
- [56] L. Ray, Neutron isotopic density differences deduced from 0.8 gev polarized proton elastic scattering, *Phys. Rev. C* **19**, 1855 (1979).
- [57] G. W. Hoffmann, L. Ray, M. Barlett, J. McGill, G. S. Adams, G. J. Igo, F. Irom, A. T. M. Wang, C. A. Whitten, R. L. Boudrie, J. F. Amann, C. Glashauser, N. M. Hintz, G. S. Kyle, and G. S. Blanpied, 0.8 gev $p+^{208}\text{Pb}$ elastic scattering and the quantity Δr_{np} , *Phys. Rev. C* **21**, 1488 (1980).
- [58] S. Abrahamyan, Z. Ahmed, H. Albatineh, K. Aniol, D. S. Armstrong, W. Armstrong, T. Averett, B. Babineau, A. Barbieri, V. Bellini, R. Beminiwattha, J. Benesch, F. Benmokhtar, T. Bielarski, W. Boeglin, A. Camsonne, M. Canan, P. Carter, G. D. Cates, C. Chen, J.-P. Chen, O. Hen, F. Cusanno, M. M. Dalton, R. De Leo, K. de Jager, W. Deconinck, P. Decowski, X. Deng, A. Deur, D. Dutta, A. Etile, D. Flay, G. B. Franklin, M. Friend, S. Frullani, E. Fuchey, F. Garibaldi, E. Gasser, R. Gilman, A. Giusa, A. Glamazdin, J. Gomez, J. Grames, C. Gu, O. Hansen, J. Hansknecht, D. W. Higinbotham, R. S. Holmes, T. Holmstrom, C. J. Horowitz, J. Hoskins, J. Huang, C. E. Hyde, F. Itard, C.-M. Jen, E. Jensen, G. Jin, S. Johnston, A. Kelleher, K. Kliakhandler, P. M. King, S. Kowalski, K. S. Kumar, J. Leacock, J. Leckey, J. H. Lee, J. J. LeRose, R. Lindgren, N. Liyanage, N. Lubinsky, J. Mammei, F. Mammoliti, D. J. Margaziotis, P. Markowitz, A. McCreary, D. McNulty, L. Mercado, Z.-E. Meziani, R. W. Michaels, M. Mihovilovic, N. Muangma, C. Muñoz Camacho, S. Nanda, V. Nelyubin, N. Nuruzzaman, Y. Oh, A. Palmer, D. Parno, K. D. Paschke, S. K. Phillips, B. Poelker, R. Pomatsalyuk, M. Posik, A. J. R. Puckett, B. Quinn, A. Rakhman, P. E. Reimer, S. Riordan, P. Rogan, G. Ron, G. Russo, K. Saenboonruang, A. Saha, B. Sawatzky, A. Shahinyan, R. Silwal, S. Sirca, K. Slifer, P. Solvignon, P. A. Souder, M. L. Sperduto, R. Subedi, R. Suleiman, V. Sulkoski, C. M. Suter, W. A. Tobias, W. Troth, G. M. Urciuoli, B. Waidyawansa, D. Wang, J. Wexler, R. Wilson, B. Wojtsekhowski, X. Yan, H. Yao, Y. Ye, Z. Ye, V. Yim, L. Zana, X. Zhan, J. Zhang, Y. Zhang, X. Zheng, and P. Zhu (PREX Collaboration), Measurement of the neutron radius of ^{208}Pb through parity violation in electron scattering, *Phys. Rev. Lett.* **108**, 112502 (2012).
- [59] I. Angeli and K. Marinova, Table of experimental nuclear

- ground state charge radii: An update, *Atomic Data and Nuclear Data Tables* **99**, 69 (2013).
- [60] K. König, J. C. Berengut, A. Borschevsky, A. Brinson, B. A. Brown, A. Dockery, S. Elhatisari, E. Eliav, R. F. G. Ruiz, J. D. Holt, B.-S. Hu, J. Karthein, D. Lee, Y.-Z. Ma, U.-G. Meißner, K. Minamisono, A. V. Oleynichenko, S. V. Pineda, S. D. Prosnjak, M. L. Reitsma, L. V. Skripnikov, A. Vernon, and A. Zaitsevskii, Nuclear charge radii of silicon isotopes, *Phys. Rev. Lett.* **132**, 162502 (2024).
- [61] J. Zhao, B.-H. Sun, I. Tanihata, J. Xu, K. Zhang, A. Prochazka, L. Zhu, S. Terashima, J. Meng, L. He, C. Liu, G. Li, C. Lu, W. Lin, W. Lin, Z. Liu, P. Ren, Z. Sun, F. Wang, J. Wang, M. Wang, S. Wang, X. Wei, X. Xu, J. Zhang, M. Zhang, and X. Zhang, Charge radii of $^{11-16}\text{C}$, $^{13-17}\text{N}$ and $^{15-18}\text{O}$ determined from their charge-changing cross-sections and the mirror-difference charge radii, *Physics Letters B* **858**, 139082 (2024).
- [62] V. Kota, Embedded random matrix ensembles for complexity and chaos in finite interacting particle systems, *Physics Reports* **347**, 223 (2001).
- [63] V. Zelevinsky and A. Volya, Nuclear structure, random interactions and mesoscopic physics, *Physics Reports* **391**, 311 (2004), from atoms to nuclei to quarks and gluons: the omnipresent manybody theory.
- [64] Y. Zhao, A. Arima, and N. Yoshinaga, Regularities of many-body systems interacting by a two-body random ensemble, *Physics Reports* **400**, 1 (2004).
- [65] H. A. Weidenmüller and G. E. Mitchell, Random matrices and chaos in nuclear physics: Nuclear structure, *Rev. Mod. Phys.* **81**, 539 (2009).
- [66] B. Sherrill and R. F. Casten, Future articles: Frontiers of nuclear structure: Exotic nuclei, *Nuclear Physics News* **15**, 13 (2005), <https://doi.org/10.1080/10506890500454675>.
- [67] C. W. Johnson, G. F. Bertsch, and D. J. Dean, Orderly spectra from random interactions, *Phys. Rev. Lett.* **80**, 2749 (1998).
- [68] Y. M. Zhao, A. Arima, N. Shimizu, K. Ogawa, N. Yoshinaga, and O. Scholten, Patterns of the ground states in the presence of random interactions: Nucleon systems, *Phys. Rev. C* **70**, 054322 (2004).
- [69] R. Bijker and A. Frank, Band structure from random interactions, *Phys. Rev. Lett.* **84**, 420 (2000).
- [70] J. J. Shen, H. Jiang, and G. J. Fu, Robustness of “noncollective” rotational behavior for nuclei in the presence of random interactions, *Phys. Rev. C* **104**, 054319 (2021).
- [71] G. J. Fu, J. J. Shen, Y. M. Zhao, and A. Arima, Regularities in low-lying states of atomic nuclei with random interactions, *Phys. Rev. C* **91**, 054319 (2015).
- [72] Y. Lei, Robust correlations between quadrupole moments of low-lying 2^+ states within random-interaction ensembles, *Phys. Rev. C* **93**, 024319 (2016).
- [73] Z.-Z. Qin and Y. Lei, Predominance of linear q and μ systematics in random-interaction ensembles, *Nuclear Science and Techniques* **29**, 163 (2018).
- [74] C. W. Johnson, W. E. Ormand, K. S. McElvain, and H. Shan, *Bigstick: A flexible configuration-interaction shell-model code* (2018), [arXiv:1801.08432 \[physics.comp-ph\]](https://arxiv.org/abs/1801.08432).
- [75] P. Karl, VII. note on regression and inheritance in the case of two parents, *Proc. R. Soc. Lond.* **58**, 240 (1895).
- [76] P. Marevic, N. Schunck, E. Ney, R. Navarro Perez, M. Verriere, and J. O’Neal, Axially-deformed solution of the skyrme-hartree-fock-bogoliubov equations using the transformed harmonic oscillator basis (iv) hfbtho (v4.0): A new version of the program, *Computer Physics Communications* **276**, 108367 (2022).
- [77] M. Dutra, O. Lourenço, J. S. Sá Martins, A. Delfino, J. R. Stone, and P. D. Stevenson, Skyrme interaction and nuclear matter constraints, *Phys. Rev. C* **85**, 035201 (2012).
- [78] L. Devroye, Multivariate distributions, in *Non-Uniform Random Variate Generation* (Springer New York, New York, NY, 1986) pp. 554–610.
- [79] H. Kohler, Skyrme force and the mass formula, *Nuclear Physics A* **258**, 301 (1976).
- [80] B. T. Reed, F. J. Fattoyev, C. J. Horowitz, and J. Piekarewicz, Implications of prex-2 on the equation of state of neutron-rich matter, *Phys. Rev. Lett.* **126**, 172503 (2021).
- [81] K. Heyde and J. L. Wood, Shape coexistence in atomic nuclei, *Rev. Mod. Phys.* **83**, 1467 (2011).
- [82] Y. Lei, J. Qi, Y. Lu, H. Jiang, Z. Z. Qin, D. Liu, and C. W. Johnson, Pervasiveness of shape coexistence in nuclear pair condensates, *Phys. Rev. C* **110**, 054318 (2024).
- [83] B. A. Marsh, T. Day Goodacre, S. Sels, Y. Tsunoda, B. Andel, A. N. Andreyev, N. A. Althubiti, D. Atanasov, A. E. Barzakh, J. Billowes, K. Blaum, T. E. Cocolios, J. G. Cubiss, J. Dobaczewski, G. J. Farooq-Smith, D. V. Fedorov, V. N. Fedosseev, K. T. Flanagan, L. P. Gaffney, L. Ghys, M. Huyse, S. Kreim, D. Lunney, K. M. Lynch, V. Manea, Y. Martinez Palenzuela, P. L. Molkanov, T. Otsuka, A. Pastore, M. Rosenbusch, R. E. Rossel, S. Rothe, L. Schweikhard, M. D. Seliverstov, P. Spagnoletti, C. Van Beveren, P. Van Duppen, M. Veinhard, E. Verstraelen, A. Welker, K. Wendt, F. Wienholtz, R. N. Wolf, A. Zadvornaya, and K. Zuber, Characterization of the shape-staggering effect in mercury nuclei, *Nature Physics* **14**, 1163 (2018).
- [84] R. P. de Groote, J. Billowes, C. L. Binnarsley, M. L. Bissell, T. E. Cocolios, T. Day Goodacre, G. J. Farooq-Smith, D. V. Fedorov, K. T. Flanagan, S. Franchoo, R. F. Garcia Ruiz, W. Gins, J. D. Holt, Á. Koszorús, K. M. Lynch, T. Miyagi, W. Nazarewicz, G. Neyens, P.-G. Reinhard, S. Rothe, H. H. Stroke, A. R. Vernon, K. D. A. Wendt, S. G. Wilkins, Z. Y. Xu, and X. F. Yang, Measurement and microscopic description of odd-even staggering of charge radii of exotic copper isotopes, *Nature Physics* **16**, 620 (2020).